Modeling Radar Propagation Over Terrain

Denis J. Donohue and James R. Kuttler

Mathematical techniques are presented for modeling electromagnetic propagation over an irregular boundary. The techniques are aimed at upgrading the Applied Physics Laboratory's Tropospheric Electromagnetic Parabolic Equation Routine (TEMPER) model for radar propagation over terrain. The physical domain with an irregular boundary is mapped to a rectangular domain, where a numerical solution can be generated by the same approach used in TEMPER. This new method is applied to several model terrain problems and shown to be accurate and practical for a reasonable range of surface slopes. Interesting results are discussed for the shadowing of radar by terrain obstacles and the detection of low-flying targets over mountainous terrain. (Keywords: Electromagnetics, Ground clutter, Parabolic equation, Propagation, Rough boundaries.)

INTRODUCTION

The propagation of radar waves at low grazing angles over terrain is a critical area for numerical modeling and performance prediction. A principal goal is estimating ground clutter, or surface backscatter, an obvious impediment to target detection. In addition, diffuse reflection from the ground can alter the coherent interference between the direct and reflected beams, adding additional uncertainty to the radar's coverage pattern. These terrain effects become even more pronounced when coupled with atmospheric refraction. The inhomogeneity of the atmosphere, which often takes the form of horizontally stratified density layers, can redirect radar energy such that repeated interaction with the ground occurs. The Theater Systems Development Group of APL's Air Defense Systems Department has developed the computational model TEMPER (Tropospheric Electromagnetic Parabolic Equation Routine) to better understand and predict the effect of such environmental factors on radar system performance.

TEMPER has been under development at APL since the early 1980s. The first objective was to accurately calculate electromagnetic propagation over the sea in complicated refractive environments.[1–5] TEMPER is currently used extensively on several Navy programs to provide propagation calculations for radar system de-

sign studies, posttest reconstruction, and *in situ* shipboard environmental assessment. Although TEMPER is mature and well established as a predictor of propagation over the sea, the Navy's current emphasis on littoral operations results in a need for accurate propagation calculations over irregular terrain as well. This article describes recent efforts to develop algorithms to address this need.

The Parabolic Wave Equation (PE) was first derived in the 1940s by Fock,[6] but analytical solutions were developed only for problems involving unrealistically simple refractive conditions. In 1973, Hardin and Tappert introduced an efficient numerical approach for solving the PE called the Fourier/split-step algorithm.[7] This algorithm was used primarily for underwater propagation until 1981, at which time Harvey Ko and colleagues in APL's Submarine Technology Department (STD) modified an acoustic model to address electromagnetic propagation in the troposphere.[1] The new model was called the Electromagnetic Parabolic Equation (EMPE).

In 1984, Dan Dockery, then in the Fleet Systems Department, working with the STD developers and members of the APL Research Center, began modifications to expand EMPE's capabilities as a radar propagation prediction tool.[2–5] These upgrades included incorporation of an impedance boundary condition, a rough surface model, and flexible antenna pattern algorithms; increased numerical efficiency and robustness were also achieved. Eventually, the model was renamed TEMPER to avoid confusion with the original program. An extensive experimental campaign was also undertaken between 1984 and 1989 to validate EMPE/TEMPER using calibrated propagation data collected in measured refractive conditions.[2,3] These tests established the accuracy of the PE Fourier/split-step approach for predicting radar propagation over the sea in complicated, range-varying, refractive environments.

At present, however, TEMPER is limited in its ability to rigorously account for irregular terrain. Accurate numerical solutions can only be guaranteed when propagating over mean smooth surfaces, such as a flat plane or spherical Earth. An approximate technique, described in the next section, was previously introduced to account for arbitrary changes in surface slope. However, this technique introduces nonquantifiable errors into the solution. This article describes techniques for rigorously incorporating an irregular boundary into the TEMPER model. A principal requirement is that the new technique allows one to retain the Fourier/split-step numerical approach. We emphasize that the terrain under consideration contains roughness features or slope variations on scales that are much larger than the typical radar wavelength λ (centimeters to meters). The effect of fine-scale roughness that is comparable to or smaller than the wavelength is particularly important to propagation over the ocean surface and to certain types of terrain as well (a related problem is scattering from ground cover/foliage). Alternative techniques have been developed to account for such features,[4] and they are not discussed here.

REVIEW OF PARABOLIC WAVE EQUATION AND FOURIER/SPLIT-STEP SOLUTION

TEMPER is based on the PE, an approximation to the reduced wave (or Helmholtz) equation, where it is assumed that the wave energy propagates predominantly in the forward or horizontal direction. This approximation has been found to work quite well for modeling low-grazing-angle radar propagation. The principal advantage of the PE approach is numerical efficiency. By neglecting backscattered wave energy and restricting propagation to small angles with respect to the horizon, highly optimized numerical methods can be employed to rapidly calculate propagation over tens or even hundreds of kilometers in range. Altitudes are generally limited to a few kilometers above the Earth's surface. The PE approach is also well suited to incorporating atmospheric refraction. Rigorous solution over a large-scale irregular boundary has previously been considered a limitation of the PE method.

For this article, we consider a scalar form of the Helmholtz wave equation, corresponding to one component of a vector electric (or magnetic) field. Furthermore, we assume azimuthal homogeneity of the atmosphere and terrain, so that solutions are generated in a two-dimensional (range x vs. altitude z) slice. Under these assumptions, the Helmholtz equation for the field ϕ has the form

$$\frac{\partial^2 \phi(x,z)}{\partial x^2} + \frac{\partial^2 \phi(x,z)}{\partial z^2} + k^2 n^2(x,z)\phi(x,z) = 0, \qquad (1)$$

where $k = 2\pi/\lambda$ is the wavenumber of the field and n is the index of refraction. It is important to emphasize that all of the effects of atmospheric refraction are incorporated into n, and furthermore, the boundary mapping methods discussed in the next section result in modification to n only. This is critical to the approach, since it allows us to account for both atmospheric and terrain effects through the standard methods used to solve Eq. 1.

To obtain the parabolic form of the wave equation, we first assume that the field ϕ propagates as time-harmonic ($e^{i\omega t}$), cylindrical (two-dimensional) waves of the form $\phi(x,z) = u(x,z)e^{i(\mathbf{k}\cdot\mathbf{r})}/\sqrt{|r|}$, where r is the distance from the source in the two-dimensional space.

The function $u(x,z)$ can be regarded as the slowly varying (in space) envelope of the propagating wave field. Our objective is a wave equation for u in which the traveling wave dependence is factored out of the problem. By substituting u into Eq. 1 and dropping a term containing $\partial^2 u(x, z)/\partial x^2$ (the paraxial approximation), we arrive at such a form,

$$\frac{\partial u(x,z)}{\partial x} = \left\{ \frac{i}{2k}\frac{\partial^2}{\partial z^2} + \frac{k}{2}[n^2(x,z) - 1] \right\} u(x,z). \qquad (2)$$

The paraxial approximation used to derive Eq. 2 assumes that the propagation is nearly horizontal, and that gradients in the horizontal direction are small compared with the vertical. For a complete development of this equation, the reader is referred to Ref. 4. Equation 2 is a parabolic partial differential equation that can be solved as an initial value problem. A starting field, $u(z)$, is specified for an initial x, and the solution is marched forward in range. The marching method is highly efficient numerically, particularly since the range and altitude stepping can be decoupled using the Fourier/split-step method. In this approach, the altitude coordinate z is paired with a Fourier transform variable p. The approximate solution at range step $x + \delta x$ is given by

$$u(x + \delta x, z) = e^{i\frac{k}{2}\int m dx}\, \mathcal{F}^{-1}\left\{ e^{-i\frac{p^2}{2k}\delta x}\, \mathcal{F}\{u(x,z)\} \right\}, \qquad (3)$$

where $\mathcal{F}$ and $\mathcal{F}^{-1}$ are the forward and inverse Fourier transforms in (z, p) space and $m = n^2 - 1$. The exponential form of the operators in Eq. 3 can be understood by considering Eq. 2 as a first-order linear differential equation in x, with a corresponding exponential solution. A solution such as Eq. 3 assumes m is very small compared with one. The smallness of m allows for the expansion of an exponential operator, which can be carried out in different ways.[8] We show Eq. 3 as one such example. These expansions must be applied cautiously when using boundary mapping methods such as those discussed in the next section. The modified m may no longer be small, particularly when the surface has large slopes or small radii of curvature.

As mentioned previously, $u(x, z)$ is the envelope function or amplitude for one component of a vector field. The standard approach is to decompose the electric field into a component that is perpendicular to the (x, z) plane of incidence (horizontal polarization or H-pol), and a component that is parallel to the plane of incidence (vertical polarization or V-pol). For a perfectly conducting and flat surface at $z = 0$, the H-pol field satisfies Dirichlet's boundary condition $[u(x, 0) = 0]$, whereas the V-pol field satisfies Neumann's boundary condition $[\partial u(x, 0)/\partial z = 0]$. These boundary conditions are satisfied exactly by using either sine (Dirichlet or H-pol) or cosine (Neumann or V-pol) transforms in Eq. 3. For nonflat surfaces, the z derivative becomes a normal derivative, which couples both x and z. In that case, satisfying the boundary condition is considerably more involved. An approach discussed in the next section is to map the irregular surface via coordinate transformation to a space in which the surface is locally flat, so that a similar splitting of cosine and sine transforms may be employed. We emphasize that once solutions are obtained for the orthogonal H and V polarizations, the solution for *any* linear polarization state may be obtained by simple linear combination.

The preceding discussion considers the solution of the PE over surfaces that are flat or that may be made flat by simple coordinate transformation. Although the following section considers more general boundaries of nonzero slope, the current TEMPER code uses an approximate technique for such boundaries that may be mentioned here. The terrain is approximated by a sequence of up and down stair steps. At each down step, the solution for the field at the new step is zero padded down to the level of the dropped terrain. At each up step, the field is trimmed off or zeroed below the level of the new (raised) terrain. This technique, called terrain blocking or masking, essentially approximates the terrain by a series of knife edges and can only be used for horizontal polarization over perfect conductors. Figure 1 shows a sample calculation generated by

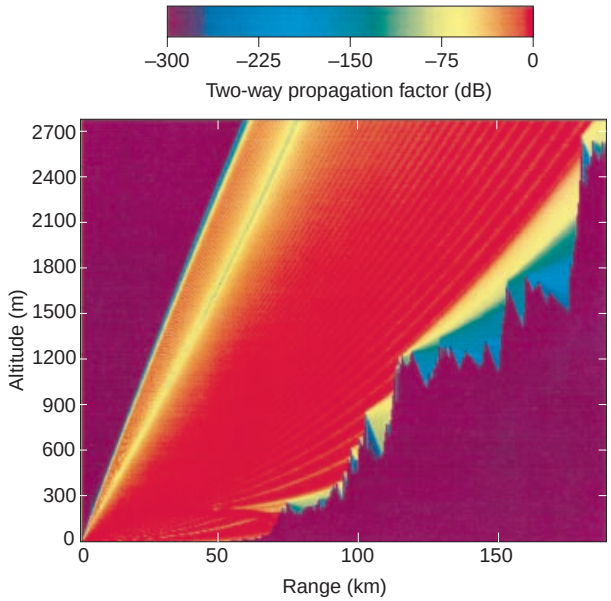

Figure 1. A sample calculation of the two-way propagation factor over digitally sampled terrain using the terrain masking approximation (f =11 GHz, V-pol). The color bar shows the mapping of field intensity. A value of 0 dB indicates the intensity that would be obtained in the absence of any terrain boundary or atmospheric refraction.

TEMPER with the terrain masking algorithm. The terrain is an actual digitized sample from a mountainous coastal region, and it represents the type of problem we wish to solve accurately using newly developed techniques. Later in the article, we compare a similar result to a more rigorous solution generated with these techniques.

TERRAIN MAPPING METHODS FOR IRREGULAR BOUNDARIES

As shown in the previous section, electromagnetic propagation is determined by solving the Helmholtz equation (Eq. 1) on a two-dimensional region S representing a vertical (x, z) plane above the surface of the Earth. When the Earth's surface is undulating, as for a regular train of waves on the sea, or has large-scale roughness, as for specific terrain features, the physical region S will have an irregular lower boundary. Our computations, however, must be carried out on a rectangular region R with a straight lower boundary.

The central theme of this article is how to map the physical domain S to the computational domain R. All of the maps we use have the important property that the Helmholtz equation (Eq. 1) on S is still a Helmholtz equation in the coordinates of R. The only modification is to the refractive index n. Thus, terrain effects as well as atmospheric effects are all accounted for in the nature of n, and the same PE Fourier/split-step method can be retained.

Let us now examine the mappings, see how they modify n, and determine how well they work. The mappings we look at are global conformal maps, piecewise conformal maps, continuous shift maps, piecewise linear shift maps, and wide-angle piecewise linear shift maps. We test them on a variety of simple domains, which are assumed to be over perfectly conducting surfaces at horizontal polarization (Dirichlet boundary). The test domains are sketched in Fig. 2. We use simple domains and boundary conditions to isolate the effects of the geometry.

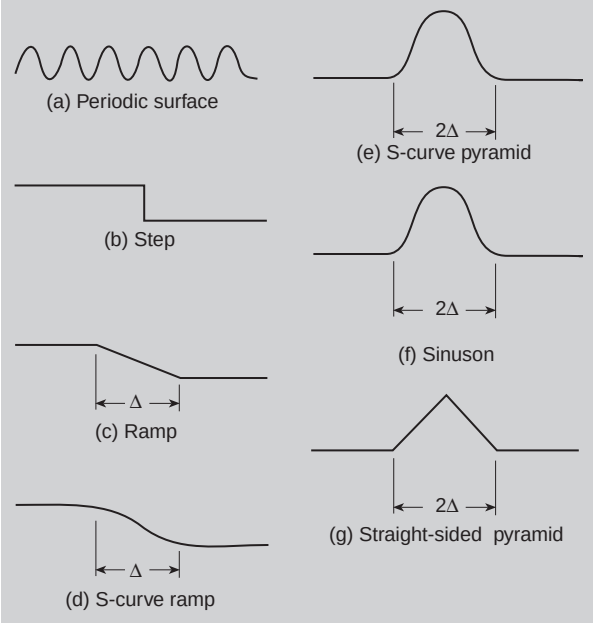

Figure 2. Various model terrain profiles. The following mapping methods were used for the profile shown in the corresponding part of the figure: (a) global conformal; (b) global conformal, exact solution; (c) global conformal, piecewise linear shift; (d) piecewise conformal, continuous shift; (e) piecewise conformal; (f) continuous shift, piecewise linear shift; (g) piecewise linear shift, wide-angle piecewise linear shift.

Global Conformal Maps

The first type of mapping we use is global conformal mapping. If $w = w(\xi)$ is a conformal map from R to S, the index of refraction n is simply multiplied by $|w'|$, the modulus of the derivative of the mapping function. As long as $|w'|$ does not differ too far from unity, the angle limitations on the parabolic approximation ($m << 1$) are satisfied, and the map works quite well in the numerical method. An illustration of a global conformal map is shown in Fig. 3. In this problem, the physical domain S, which is bounded by a curved ramp, is mapped to the rectangular computational domain. The distortion introduced by the mapping to the area of the rectangular cells is a measure of $|w'|$.

The global conformal mapping method is applied to a regular train of waves on the sea, as shown in Fig. 2a. For an ocean wavelength of 344 m and amplitude of 4 m, the waves have sufficiently gentle slopes that the requirement on $|w'|$ is met. This surface is illuminated by a 25.6-MHz broadband antenna placed so high (5.3 km) that it simulates a plane wave at the surface. The result is Bragg scattering,[9] which is a superposition of plane waves at angles determined by the grating law (see Fig. 4).

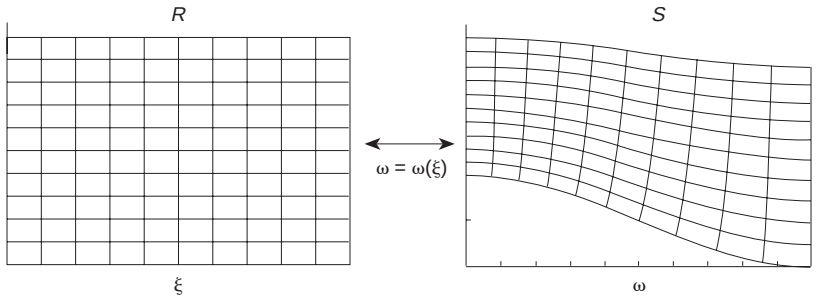

Figure 3. An example of a conformal map [$w = w(\xi)$] from the computational domain R (left) to the physical domain S (right).

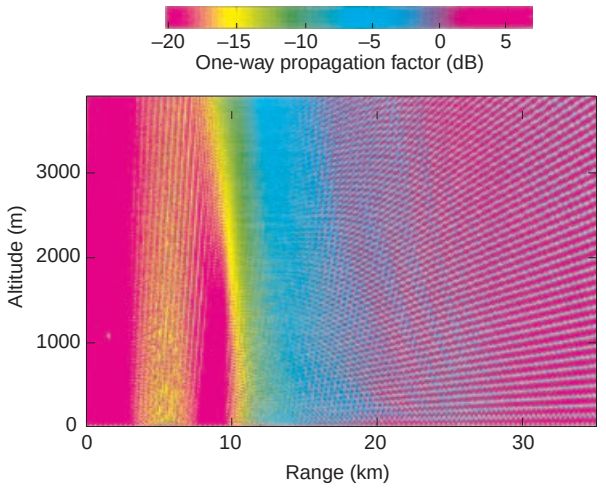

Figure 4. Propagation over a train of ocean waves calculated by the global conformal mapping method (f = 25.6 MHz, H-pol). The result shows the onset of Bragg scattering from the periodic surface.

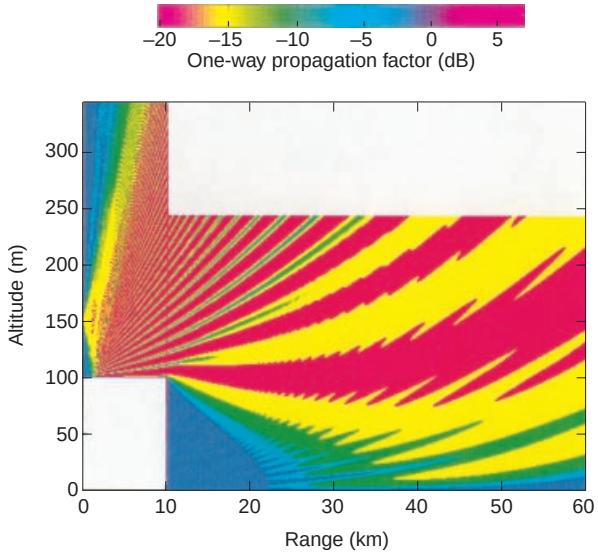

Figure 5. Propagation over a 100-m step calculated exactly by the superposition of two rectangular domains (f = 3 GHz, H-pol). A deep shadowing of the field is observed behind the step in the range of 10–30 km. This result is used as a benchmark for the various terrain mapping methods.

Although conformal maps can be easily found for the steps and ramps shown in Figs. 2b and 2c, the gradients in such mappings are so steep that $|w'|$ becomes too large, and the angle restrictions on the parabolic equation are violated. The step problem can actually be solved exactly by a simple trick. The problem is solved on two rectangular regions. The PE propagates from left to right in the first rectangle, starting from the given antenna pattern [the initial value $u(0, z')$]. To continue from the first rectangle to the second, the field is padded at the bottom with as many zeros as correspond to the height of the step, and the same number of points are trimmed off the top. This shifted field is then used as the starting field for the second rectangle, and the field is again propagated to the right. This method gives the true solution for the step problem, which we are able to use as a benchmark to test other terrain mapping methods. The case of a 3-GHz antenna at 50 m above the surface and a 100-m step at 10 km from the antenna is shown in Fig. 5. Field strength in decibels is color plotted. The ramp problems of Figs. 2c and 2d have been solved by conformal mapping and compared with Fig. 5. When the width Δ of the ramp is moderately small, the solution is essentially the same as that for the step. What we do is use a mapping method on a ramp problem and decrease Δ until the method fails. Failure can be seen (in plots like Fig. 5) when the diffraction no longer goes smoothly over the top edge of the ramp. The onset of failure is detected when the locations of the nulls in horizontal cuts through the field begin to move away from their correct location. This condition tells us the limitation on the terrain slopes that the method can handle correctly.

Piecewise Conformal Maps

The next type of mapping used is piecewise conformal mapping. The physical region is broken up into a number of separate pieces, each of which is mapped to its own rectangular computational region. The computed field must be handed off from each computational region to the next one by using a forward map, an interpolation, and an inverse map. Again, the index of refraction n is simply multiplied by $|w'|$, but w differs from region to region. Dozier[10] previously used a piecewise conformal map that takes rectangular strips to strips with straight, angled ends. These maps use elliptic integrals and are computationally intensive. We used a simpler map of the form $w = \log(c + e^{ibz})$, where the parameters c and b adjust the shape of the map. This map takes rectangular strips to strips with S-curve ends and has the advantage that its inverse is of the same form. We used this map for the curved ramp of Fig. 2d. The gradients in this mapping are much more gradual than in the global conformal maps, and we are able to use S-curves of height 100 m and widths down to 1 km before the method begins to fail. These dimensions correspond to a slope of 1:10 or about 5.7°. Again, the overall result is very similar to the step problem of Fig. 5. We also considered the curved pyramid problem of Fig. 2e by piecewise conformal maps. On a sample problem, the results were found to be accurate for pyramid slopes as large as about 6.5°, which is apparently the limit of the piecewise conformal mapping approach.

Continuous Shift Maps

The next mapping considered, the continuous linear shift, was first introduced by Beilis and Tappert.[11] Given a surface profile described by a function $z = T(x)$, the problem may be mapped to the rectangular domain R by the continuous coordinate transformation

$$x' = x, \qquad z' = z - T(x) \; . \tag{4}$$

Beilis and Tappert also showed that by replacing the amplitude function $u(x, z)$ with $\bar{u}(x', z')e^{i\theta(x', z')}$, and by making an appropriate choice for the function θ, then a modified PE of the form of Eq. 2 can be derived. In the modified PE, the refractivity term becomes $\bar{m} = n^2 - 1 - 2z'd^2T/dx'^2$, that is, the index of refraction is modified by a new term proportional to the rate of change of slope of the surface. The shift map is particularly attractive for our application, since the exact same method used in TEMPER for the solution of the PE may be employed. Moreover, for the Dirichlet boundary, the only required addition to the TEMPER algorithm is the modification of the refractive index. The shift map is also mathematically rigorous in that no additional approximations are made beyond those that are required in the derivation of the PE.

The shift map was first tested on the ramp of Fig. 2c.[12] The result compares well with Fig. 5, which gives a measure of confidence in the numerical accuracy of the approach. A new problem considered with the shift map is the straight-sided pyramid of Fig. 2g. A sample result is shown in Fig. 6. In this example, an H-pol 3-GHz antenna is located 30.5 m above the ground. The pyramid begins 10 km downrange of the antenna and has a base dimension of 20 km and a height of 229 m.

We also applied the shift map to the sinuson of Fig. 2f, a continuously curved profile having an analytical and continuously differentiable representation for $T(x)$. Propagation over the sinuson is illustrated in Fig. 7. The sinuson has a base dimension of 20 km and a height of 229 m, so that its overall physical dimensions are comparable to the sharply peaked pyramid shown in Fig. 6. An important difference between these two results is the shadowing of the incident field behind the model terrain obstacle. Over the smoothly curved sinuson, the shadowing is very nearly geometric; that is, the field strength is significantly reduced behind the obstacle, and the shadow zone follows a roughly geometric form bounded by a line joining the antenna with the peak of the obstacle. In the pyramid problem, significantly greater field strengths are observed behind the obstacle. The elevated field strengths extend well into the geometric shadow zone. The important difference between the two problems is the sharp peak of the pyramid, which acts as a diffraction wedge. When propagating over sharp corners or edges, geometrical optics is a poor approximation. As Fig. 6 shows, the problem can be diffraction dominated.

The sharp contrast between Figs. 6 and 7 is significant for propagation modeling over terrain. In particular, the shadowing of the radar is strongly dependent on both the height and the peakedness, or radius of curvature, of the terrain. When working with sampled terrain data, the curvature information may not be available. It is therefore critical to know whether accurate propagation predictions can be based solely on terrain elevation samples, and if so, how finely the

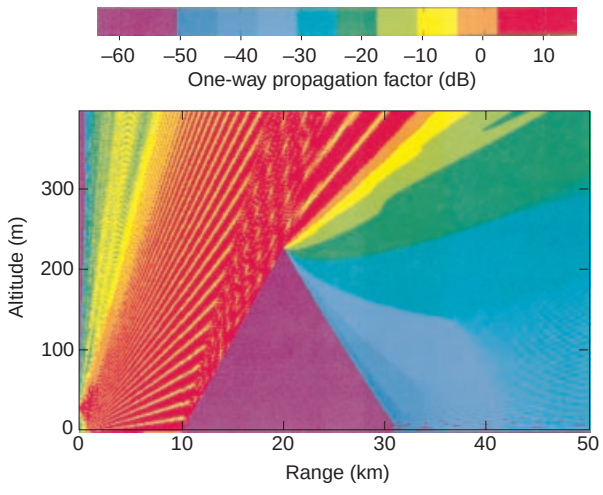

Figure 6. Propagation over a 229 m × 20 km pyramid calculated by the piecewise linear shift map (f = 3 GHz, H-pol). Note the strong reflections off the front face of the pyramid and the diffraction of the field by the vertex.

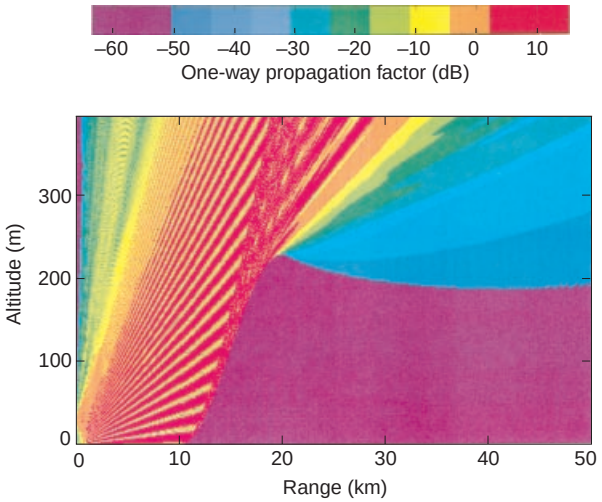

Figure 7. Propagation over a 229 m × 20 km sinuson profile calculated by the piecewise linear shift map (f = 3 GHz, H-pol). The shadow region, behind the terrain obstacle, is markedly different than in Fig. 6.

terrain must be sampled to minimize modeling errors. For example, surface-based radar detection of low-flying targets in the shadow zone may be hampered by low signal-to-noise ratios. Under such conditions, a difference of perhaps 5–10 dB in signal strength could determine if a target is detectable at all.

Piecewise Linear Shift Maps

To examine modeling with sampled terrain, we have developed an adaptation of the continuous shift map that we call the piecewise linear shift map. The terrain is represented by connected piecewise linear segments, as might be obtained by joining terrain elevation samples by straight lines. The piecewise linear shift map tracks the change in surface slope *discretely* at each segment boundary, as opposed to the *continuous* integration of the rate of change of slope in the shift map algorithm. This method was tested over a piecewise linear representation of the sinuson profile of Fig. 7. For example, a sample result used eight linear segments to span the 20-km-long terrain obstacle, so that the elevation samples were separated by 2.5 km. The PE code was run with a range step ($\Delta x'$) of 100 m, which is small compared with the surface sampling. As might be expected, the shadow zone was intermediate in size to Fig. 6 (the sharp peak) and Fig. 7 (the smoothly curved sinuson). Again, this result is due to the intermediate peakedness of the sampled sinuson. The sharp peak may be removed either by interpolating the samples and returning to a continuously curved representation of the surface ($T'' \neq 0$), or by retaining the piecewise linear representation but sampling on a finer scale. Since the piecewise linear approach has several advantages, including simplicity, we also examined the problem with various sampling rates. A simulation using a rate of 1 surface sample every 10 range steps was found to be virtually indistinguishable from the exact result (Fig. 7). This finding confirms the utility of the piecewise linear approach for sampled terrain. However, the accuracy will depend strongly on a sufficient sampling interval to represent the actual curvature of the terrain.

When using a continuously curved representation of the surface, perhaps through interpolation or curve fitting of the terrain data, integration rules must be used that are appropriate for the curvature of the surface. Specifically, Eq. 3 shows m is integrated over range in the left-hand exponential term. In many cases, a simple approximation such as the trapezoid rule may be used. However, the shift-map algorithm introduces the term T'' into m. If the surface is sharply curved on the scale of the range step (Δx), the trapezoid rule can introduce a sizable error. Higher-order integration rules, such as Gaussian quadrature, may overcome this problem. In some cases, a smaller range step may be required. Another possibility is an adaptive range-stepping algorithm where Δx is dynamically determined on the basis of an appropriate error criterion.

Wide-Angle Piecewise Linear Shift Maps

As mentioned previously, many approximate Fourier/split-step solutions to the PE can be derived on the basis of expansions of an exponential operator. The simplest form, shown in Eq. 3, is referred to as the narrow-angle result, since it is the most strongly limited in the acceptable range of propagation angles about the horizontal. More robust wide-angle forms[8] have been derived and used in TEMPER for propagation over a rectangular domain. Recently, we developed a new wide-angle version of the piecewise linear shift map. This improved algorithm was tested on the straight-sided pyramid (Fig. 2g) and found to give acceptable results for Δ as small as about 1 km, corresponding to surface slopes as large as 12.9°. The wide-angle piecewise linear shift map has therefore been identified as the most robust mapping method studied in terms of allowable surface slope, and it is most straightforward to employ within the TEMPER algorithm. We remark that a larger transform size was needed for smaller Δ to avoid a grating lobe error at the vertex of the pyramid.

Now that we have reviewed the shift map algorithm, it is interesting to compare this more rigorous technique with the terrain masking algorithm discussed in the previous section. An example is shown in Fig. 8. Both results assume Dirichlet boundary conditions, which are required for the terrain masking approximation. Although the two results appear similar, some important differences exist. In the shift map solution, there are strong reflections of the incident field off of the front faces of the pyramids. Terrain masking ignores reflections entirely; the weak fields radiating from the front faces of the pyramids result from approximating the terrain by a series of knife-edge diffractors. The two results also differ in signal strength in the troughs between pyramids, particularly in the latter two. Differences as large as 5–10 dB can be observed deep in the troughs.

Computing Requirements

The results shown in this article typically require several minutes of computing time to generate on a late-model desktop workstation. The most detailed simulations (large transform size and small range step) require on the order of 1 h. The time requirement for a typical personal computer is longer, but still practical. Since the calculations are two-dimensional, the memory requirement is quite reasonable. The calculated field on the two-dimensional grid occupies most of the required memory; however, in most cases, only a small fraction of the calculated values needs to be retained for analysis and display.

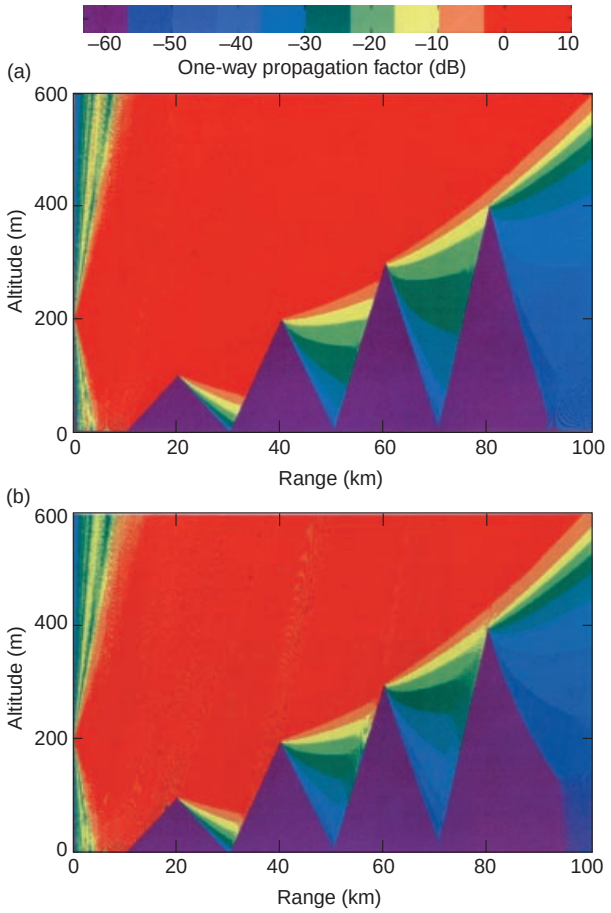

Figure 8. A comparison of (a) the terrain masking approximation to (b) the piecewise linear shift map, on a model problem.

Finally, our more recent work on this problem has focused on polarization dependence and (finite) surface electrical parameters. A special technique called the mixed Fourier transform has been developed at APL for the TEMPER code.[4,5] This technique, based on the Leontovich boundary condition (which couples the field and its normal derivative on the surface), introduces both finite surface conductivity and horizontal/vertical polarization dependence. As mentioned earlier, a tilted boundary couples range and altitude gradients when taking the normal derivative of the field. In that case, the solution of the Leontovich boundary condition in the PE is considerably more involved than over a rectangular domain. We have taken two approaches to this problem as part of the shift map. First, a complete mathematical solution has been developed that will be reported in a later publication. A second approach is to approximate the new boundary condition under the assumption of small surface slope. This method has been tested for both polarizations on various problems, including the actual terrain sample shown in Fig. 1. One of the preliminary findings is that for a reasonable range of ground permittivity and conductivity values, propagation at H-pol is weakly dependent on the electrical parameters. At higher radar frequencies (3–30 GHz) and typical ground electrical parameters, the H-pol and V-pol results also tend to be quite similar. At lower (HF) frequencies (3–30 MHz), V-pol propagation becomes strongly dependent on the electrical properties. In this range, surface wave effects, which are included in the mixed Fourier transform approach, become important. More extensive calculations of HF propagation and ground effects are currently under way.

SUMMARY

We have analyzed several techniques for solving the PE over an irregular boundary. The mathematically rigorous approach is to map the irregular domain to a rectangular domain, where well-established numerical methods can be used. The mapping methods are applied to radar propagation modeling over terrain. By analysis of several model terrain profiles, we have identified the wide-angle piecewise linear shift as the most robust mapping in terms of the allowable range of surface slopes. This mapping should be useful for a wide range of practical terrain problems. A full solution has been developed incorporating polarization dependence and finite surface electrical parameters. The numerical methodology is similar to that used in the TEMPER propagation model and therefore will be a straightforward addition to TEMPER.

In the future, we plan to combine the terrain mapping method with fine-scale roughness effects such as vegetation scatter, and with the varying electrical properties of different soil and vegetation types as well as snow/ice cover. An overriding goal is a high-fidelity predictive model for radar ground clutter. Given the important contribution of both atmospheric refraction and surface interaction, the PE with surface mapping appears to be an excellent approach for such a model.

REFERENCES

[1]Ko, H. W., Sari, J. W., and Skura, J. P., "Anomalous Microwave Propagation Through Atmospheric Ducts," *Johns Hopkins APL Tech. Dig.* **4**, 12–26 (1983).
[2]Dockery, G. D., and Konstanzer, G. C., "Recent Advances in Prediction of Tropospheric Propagation Using the Parabolic Equation," *Johns Hopkins APL Tech. Dig.* **8**, 404–412 (1988).
[3]Dockery, G. D., *Description and Validation of the Electromagnetic Parabolic Equation Propagation Model (EMPE)*, Fleet Systems Department Report, FS-87-152, JHU/APL, Laurel, MD (Sep 1987).
[4]Kuttler, J. R., and Dockery, G. D., "Theoretical Description of the Parabolic Approximation/Fourier Split-Step Method of Representing Electromagnetic Propagation in the Troposphere," *Radio Sci.* **26**, 381–393 (1991).
[5]Dockery, G. D., and Kuttler, J. R., "An Improved Impedance Boundary Algorithm for Fourier Split-Step Solutions of the Parabolic Wave Equation," *IEEE Trans. Ant. Prop.* **44**(12), 1592–1599 (1996).
[6]Fock, V. A., "Solution of the Problem of Propagation of Electromagnetic Waves Along the Earth's Surface by Method of Parabolic Equations," *J. Phys. USSR* **10**, 13–35 (1946).

[7]DiNapoli, F. R., and Deavenport, R. L., "Numerical Methods of Underwater Acoustic Propagation," in *Ocean Acoustics*, J. A. DeSanto (ed.), Springer-Verlag, pp. 135–137 (1977).
[8]Jensen, F. B., Kuperman, W. A., Porter, M. B., and Schmidt, H., *Computational Ocean Acoustics*, AIP Press, New York (1994).
[9]Kuttler, J. R., and Huffaker, J. D., "Solving the Parabolic Wave Equation with a Rough Surface Boundary Condition," *J. Acoust. Soc. Am.* **94**, 2451–2454 (1993).
[10]Dozier, L. B., "PERUSE: A Numerical Treatment of Rough Surface Scattering for the Parabolic Wave Equation," *J. Acoust. Soc. Am.* **75**, 1415–1432 (1984).
[11]Beilis, A., and Tappert, F. D., "Coupled Mode Analysis of Multiple Rough Surface Scattering," *J. Acoust. Soc. Am.* **66**, 811–826 (1979).
[12]Donohue, D. J., "Propagation Modeling Over Terrain by Coordinate Transformation of the Parabolic Wave Equation," in *Proc. 1996 IEEE Ant. Prop. Int. Symp.*, Baltimore, MD, p. 44 (Jul 1996).

ACKNOWLEDGMENTS: The authors would like to thank Dan Dockery for providing a brief history of TEMPER code development and Jeff Smoot for providing Fig. 1.

THE AUTHORS

DENIS J. DONOHUE received a B.A. in computer science from Rutgers University in 1985 and a Ph.D. in electrical engineering from Stanford University in 1991. Following a postdoctoral appointment in space plasma physics, he joined the Milton S. Eisenhower Research and Technology Development Center at APL in 1993, where he is currently a member of the Physics, Modeling, and Applications Group. Dr. Donohue's research interests span a broad range in space science and astrophysics, optics, acoustics, and electromagnetic theory. Common themes underlying all of his work are the interaction of waves (electromagnetic, acoustic, plasma) with matter, and the use of computational methods as tools for analytical research. His e-mail address is Denis.Donohue@jhuapl.edu.

JAMES R. KUTTLER is a member of the Principal Professional Staff in the Theater Systems Development Group of the Air Defense Systems Department. He received a B.A. degree in mathematics from Rice University in 1962, an M.A. degree in 1964, and a Ph.D. degree in 1967 in applied mathematics from the University of Maryland. He began working at APL as a summer student in 1963 and has been full-time since 1967. He also teaches applied mathematics courses in the Part-Time Programs of the G.W.C. Whiting School of Engineering. Dr. Kuttler has worked on synthetic aperture radar, chemical phase transitions, signal processing, fast convolution algorithms, and electromagnetic propagation and scattering models. His e-mail address is James.Kuttler@jhuapl.edu.